Magnetic cooling by the application of external pressure in rare-earth compounds

Th. Strässle* and A. Furrer
Laboratory for Neutron Scattering, ETH Zurich & PSI, 5232 Villigen PSI, Switzerland

Z. Hossain and Ch. Geibel
Max-Planck Institut für Chemische Physik fester Stoffe, 01187 Dresden, Germany
(Received 26 July 2002; published 6 February 2003)

A method for cooling by the application of pressure was recently proposed. As in any other (magnetic) adiabatic cooling technique, the cooling results from a change in the magnetic entropy of the system under investigation. As opposed to the well known method of adiabatic demagnetization (for paramagnets) or to the magnetocaloric effect (for ferromagnets and antiferromagnets), the entropy change does not result from the application of an external magnetic field, but from the application of external pressure (barocaloric effect). The pressure-induced change in the magnetic entropy may be obtained by different mechanisms including pressure-induced structural or/and magnetic phase transitions, pressure-induced changes in the degree of $4f$-conduction electron hybridization in Kondo systems, pressure-induced valence transitions, and pressure-induced spin fluctuations. The present work illustrates this new concept of adiabatic cooling on the basis of recent experimental data. The data are discussed within a simple model balancing the total entropy as a function of microscopic thermodynamic parameters of the system under investigation. Implications for a possible technical use of this effect are addressed.

DOI: 10.1103/PhysRevB.67.054407 PACS number(s): 75.30.Sg, 65.40.Gr, 62.50.+p, 71.70.Ch

I. INTRODUCTION

Ever since Warburg (1881) first observed the heat evolution in iron upon the application of a magnetic field, the so-called magnetocaloric effect (MCE) has been subject of intensive investigation. The effect is a consequence of the variation in the total entropy of a solid by the magnetic field. It was first Debye (1926) and Giauque (1927) who proposed the principle of adiabatic cooling, or more specifically the technique of adiabatic demagnetization. In the first stage, an external magnetic field is applied isothermally (the system is in contact with a heat sink), thus reducing the magnetic entropy of the system. In the second stage, the magnetic field is removed adiabatically (the system is isolated from the heat sink). In order to keep the entropy unchanged, the system is forced to lower the temperature. Progress in the theoretical as well as experimental characterization of the magnetothermal properties of materials has renewed the interest in the investigation of the MCE for two reasons: (i) the MCE can yield information on magnetic phase transitions not obtainable by other experimental techniques, and (ii) its potential for the implementation of magnetic cooling machines (magnetic refrigerators).[1] These days, magnetic refrigeration proved to be one of the most efficient cooling techniques in a wide range of temperatures up to room temperature and above.[2–4] Up to now, all magnetic refrigerators suffered the drawback of needing large magnetic fields of a few T in order to achieve cooling effects in the K range.

Despite the fact that the entropy change need not be induced exclusively by an external magnetic field, its implementation by variation of a different external thermodynamic variable has hardly been investigated. Müller *et al.*[5] proposed to implement adiabatic cooling by the application of pressure in the vicinity of a pressure-induced structural phase transition in a rare-earth compound. A pressure-induced structural phase transition will change the point symmetry at the rare-earth ion. In general this will result in a different splitting of its $(2J+1)$-fold degenerate ground-state J multiplet by the crystal field (CEF), which governs the thermodynamic properties of the system at low temperatures. Hence the external pressure p may well serve to change the magnetic entropy in the very same way as an external magnetic field does in the MCE. In analogy to the magnetocaloric effect, the associated effect has been given the name barocaloric effect (BCE). Other mechanisms equally resulting in a pressure-induced change of the magnetic entropy exist for which examples will be given below.

In what follows we briefly discuss the general thermodynamics underlying the BCE in analogy to the MCE. Models for the calculation of the total entropy of rare-earth compounds are introduced which allow one to calculate the expected BCE on the basis of microscopic parameters of the system under investigation. We compare these models with actual direct measurements of the BCE obtained in the rare-earth compounds CeSb, HoAs, $Ce_3Pd_{20}Ge_6$, and $EuNi_2(Si,Ge)_2$. In Sec. IV we compare our results obtained by the BCE with the MCE and future developments and improvements are discussed.

In the BCE, the extensive caloric effects (i.e., the change of magnetic entropy ΔS upon isothermal pressure change) are found to be comparative in size to the values found for many of the rare-earth compounds by means of the MCE. The directly observed intensive caloric effects (i.e. the change of temperature ΔT upon adiabatic pressure change) are found to be less than theoretically expected as a consequence of nonfully adiabatic conditions of the experimental setup. This fact remains an inherent problem of the proposed concept of cooling, which to a large extent may be improved as compared to the present experimental setup. Eventually, it is the value of the entropy change ΔS which in terms of

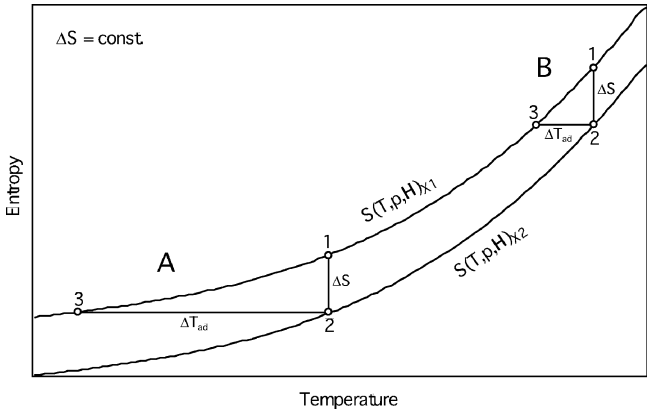

FIG. 1. A schematic of adiabatic cooling. The adiabatic temperature change ΔT_{ad} strongly depends on the slope of $S(T,p,H)$ the (isothermal entropy change $\Delta S_{X_1 \to X_2}$ is kept constant).

magnetic refrigeration in combination with a regenerator (see below) represents the crucial value which is subject to be optimized.

II. THEORY

A. General thermodynamics

As any other adiabatic cooling technique the BCE takes advantage of the fact that the total entropy S of a solid constitutes a thermodynamic state function depending on thermodynamic variables like the temperature T, pressure p, and magnetic field H; hence

$$dS = \left(\frac{\partial S}{\partial T}\right)_{p,H} dT + \left(\frac{\partial S}{\partial p}\right)_{T,H} dp + \left(\frac{\partial S}{\partial H}\right)_{T,p} dH. \tag{1}$$

Apparently, varying only one of the external variables p or H, denoted as the *control variable* X, and keeping the temperature T and the other variable K (H or p) constant, leads to a change in entropy [Eq. (1)] (Fig. 1, step $1 \to 2$):

$$\Delta S = S(T,X_2,K) - S(T,X_1,K) \tag{2}$$

$$= \int_{X_1}^{X_2} \left(\frac{\partial S(T,X,K)}{\partial X}\right)_{T,K} dX. \tag{3}$$

The extensive quantity ΔS upon an isothermal change of H is given the name extensive MCE; hence in the general case we may call ΔS the *extensive caloric effect*.

Subsequent adiabatic change of X from X_2 back to X_1 leads to a change in temperature ΔT_{ad} as the total entropy must be conserved (Fig. 1, step $2 \to 3$):

$$S(T,X_2,K) = S(T+\Delta T_{ad},X_1,K). \tag{4}$$

Accordingly the intensive quantity ΔT_{ad} is given the name *intensive caloric effect*. Recalling the second law of thermodynamics,

$$\left(\frac{dS(T,X,K)}{dT}\right)_{X,K} = \left(\frac{C(T,X,K)}{T}\right)_{X,K}, \tag{5}$$

with C denoting the total heat capacity of the system, ΔT_{ad} may be written [Eq. (3)]

$$\Delta T_{ad} = \int_{X_2}^{X_1} \left(\frac{T}{C(T,X,K)} \frac{\partial S(T,X,K)}{\partial X}\right)_{T,K} dX. \tag{6}$$

The intensive and extensive caloric effects are coupled via the adiabatic equation (4):

$$S(T,X_2,K) = S(T,X_1,K) + \frac{\partial S}{\partial T}\Big|_{X,K} \Delta T_{ad} + O(\Delta T_{ad}^2). \tag{7}$$

For ΔT_{ad} follows in first order (i.e., assuming $S \propto T$),

$$\Delta T_{ad} = \frac{\Delta S(T,X,K)_{X_1 \to X_2}}{\partial S(T,X,K)/\partial T}, \tag{8}$$

and with $C = T(\partial S/\partial T)$ [Eq. (5)],

$$\Delta T_{ad} = \Delta S(T,X,K)_{X_1 \to X_2} \frac{T}{C(T,X,K)}. \tag{9}$$

The same result is obtained by linearization of Eq. (6) (i.e., assuming $C \equiv$ const). These strong assumptions are hardly justified in any real system; nevertheless Eq. (9) has some important consequences valid for nonlinear cases too: (i) $\Delta T_{ad} \propto \Delta S$; large intensive caloric effects require large extensive caloric effects. (ii) $\Delta T_{ad} \propto T/C$; the intensive caloric effect is large for either very low T as $C \to 0$ ($T \to 0$) or for high T as $C \to$ const (T high enough). The fact $\Delta T_{ad} \propto 1/C$ is also depicted in Fig. 1. For more quantitative conclusions the specific relation of the entropy on the control variable X [i.e., $\partial S/\partial X$ in Eq. (3)] must be considered.

In the BCE and in elastic heating/cooling the entropy change ΔS is caused by external pressure p being the control variable X. In principle, as in the MCE we may take use of the Maxwell relations, i.e.,

$$\left(\frac{\partial S}{\partial p}\right)_{T,H} = -\left(\frac{\partial V}{\partial T}\right)_{p,H}, \tag{10}$$

and Eqs. (3) and (6) become

$$\Delta S = -\int_{p_1}^{p_2} \left(\frac{\partial V}{\partial T}\right)_{p,H} dp, \tag{11}$$

$$\Delta T_{ad} = -\int_{p_2}^{p_1} \left(\frac{T}{C(T,p,H)} \frac{\partial V(T,p,H)}{\partial T}\right)_{p,H} dp. \tag{12}$$

From these equations the change of volume appears as the source for the BCE (in analogy to the change of bulk magnetization in the MCE[1]). It is noteworthy to address a few important remarks at this point. The Maxwell relation [Eq. (10)] is strictly valid for constant magnetization and constant magnetic field only. Hence Eq. (10) is of limited, practical use for the BCE, as opposed to the MCE, where the corresponding relation $\partial S/\partial H = \partial M/\partial T$ represents the basis of indirect determinations of ΔS and ΔT_{ad}.[1,6,7] Nevertheless Eq. (10) may be used in the case of elastic heating/cooling or of

purely structurally and valence driven BCE, respectively (see below). The continuation of the formalism of macroscopic thermodynamics on general grounds is not being pursued any further here. We note however, that in analogy to the MCE, the extensive BCE may be determined indirectly by integration of C, i.e.,

$$\Delta S_{p_1 \to p_2} = \int_0^T \frac{C(T,p_2) - C(T,p_1)}{T} dT. \tag{13}$$

The intensive BCE ΔT_{ad} may then be calculated via Eq. (4). However, this indirect determination of the caloric effect is of less practical importance for the BCE as opposed to the MCE, too, because quantitative data of C at $p>0$ is scarce. We will thus focus on the direct experimental observation of the intensive BCE ΔT and its modeling on the basis of Eq. (4) balancing the total entropy of the system.

B. Modeling of $S(T,p)$

Equation (4) balances the total entropy

$$S = S_m + S_e + S_l, \tag{14}$$

with S_m, S_e, and S_l the magnetic, electronic and phononic contributions, respectively. Here we discuss the case of rare-earth compounds only, for which the magnetic entropy S_m is determined by the $2J+1$ CEF split energy levels of the ground-state J multiplet of the rare-earth ions,

$$S_m \simeq S_{\mathrm{CEF}} = -Nk \sum_i p_i \ln p_i, p_i = \frac{1}{Z} e^{-E_i/kT}, \tag{15}$$

with Z the partition function, N the total number of rare-earth ions in the system, and p_i the thermal population factors of the energy levels E_i. The latter are determined by the Hamiltonian

$$\hat{\mathcal{H}} = \hat{\mathcal{H}}_{\mathrm{CEF}} + \hat{\mathcal{H}}_{\mathrm{exch}} = \sum_{n,m} B_n^m \hat{O}_n^m - g_J \mu_B [(\mathbf{H}_{ex} + \lambda_D \langle \hat{\mathbf{J}} \rangle) \hat{\mathbf{J}} + \lambda_Q (\langle \hat{O}_2^0 \rangle \hat{O}_2^0 + 3 \langle \hat{O}_2^2 \rangle \hat{O}_2^2)], \tag{16}$$

with B_n^m and $\hat{O}_n^m$ the Stevens CEF parameters and operators, respectively. $\mathbf{H}_{ex}$ is an external magnetic field, and λ_D and λ_Q are the mean-field parameters for isotropic bilinear and biquadratic exchange.

For low temperatures the electronic entropy S_e may be taken to be linear in T,

$$S_e = \gamma T, \tag{17}$$

with γ the Sommerfeld factor. At low temperatures the lattice entropy may be obtained by integration of C_l [Eq. (13)] in the Debye approximation,

$$C_l(T) = 9Nk \left(\frac{T}{\Theta_D} \right)^3 \int_0^{\Theta_D/T} \frac{x^4 e^x}{(e^x - 1)^2} dx \to \frac{12\pi^4}{5} Nk \left(\frac{T}{\Theta_D} \right)^3 = \beta T^3, \quad T \ll \Theta_D, \tag{18}$$

with N the number of atoms in the system and Θ_D the Debye temperature.

We may now discuss the pressure dependence of these three entropy terms. The effect of pressure upon S_l is most familiar, and results in elastic heating and cooling, respectively. Pressure generally leads to an increase in the stiffness of the lattice and the phonon density of states is shifted to higher energies. In the Debye approximation this shift results in a scaling of Θ_D with volume V,

$$\Theta_D(V) = \Theta_D(V_0) \left(\frac{V_0}{V} \right)^{\Gamma}, \tag{19}$$

with Γ the (phononic) Grüneisen parameter defined by this relation. The intensive caloric effect ΔT_{ad} may be calculated with the adiabatic equation (4) via Eqs. (18) and (19), or by means of Eq. (12) using the thermal expansion coefficient $\alpha = 1/V(\partial V/\partial T)$ and the relation $(\alpha B V = \Gamma C)_{V,H}$, with B the isothermal bulk modulus:

$$\Delta T_{ad} = \int_{p_2}^{p_1} T \frac{\Gamma}{B} dp \approx T \frac{\Gamma}{B} \Delta p. \tag{20}$$

At low temperature the elastic heating, i.e., cooling, is thus found to be linear both in pressure and temperature. The magnitude of elastic heating in solids is of the order of typically a few 10 mK/0.1 GPa hydrostatic pressure for $T < 20$ K. The effect of pressure upon the electronic term S_e may be neglected for most of the compounds presented below, except for the important case of heavy-fermion compounds, e.g., in Kondo systems where the application of pressure generally results in a strengthening of the $4f$-conduction electron hybridization and hence to larger γ.

C. Implementations of the BCE

We shall restrict the term *barocaloric effect* to a change ΔS or ΔT upon pressure-induced changes of the *magnetic entropy* S_m only. In rare-earth compounds, S_m is dominated by the CEF entropy S_{CEF} [Eq. (15)] which is determined by five major factors: (i) the specific type of rare-earth ion, (ii) the point-symmetry of the rare-earth site, (iii) the charges of the ligands and the rare-earth ion, (iv) the screening of the charges and the degree of $4f$ hybridization due to conduction electrons, and (v) a superimposed Zeeman splitting due to an internal or external magnetic field. The application of external pressure may influence these factors in a direct manner. A pressure-induced structural phase transition may affect (ii), the associated effect may be called a structurally driven BCE. On the other hand a pressure-induced magnetic phase transition implies an internal magnetic field resulting in large Zeeman splitting (v) which in many cases is comparatively larger than by externally applied magnetic fields. The magnetically driven BCE may hence be considered the analogue to the MCE. Further, many Kondo systems show a distinct pressure dependence in the degree of $4f$ conduction electron hybridization, and hence allow for a cooling (iv). Finally, we may even realize cooling by the virtual exchange of the type of rare-earth ion (i) via a pressure-induced valence transition, e.g., $Eu^{2+} \to Eu^{3+}$. All of the above described mechanisms

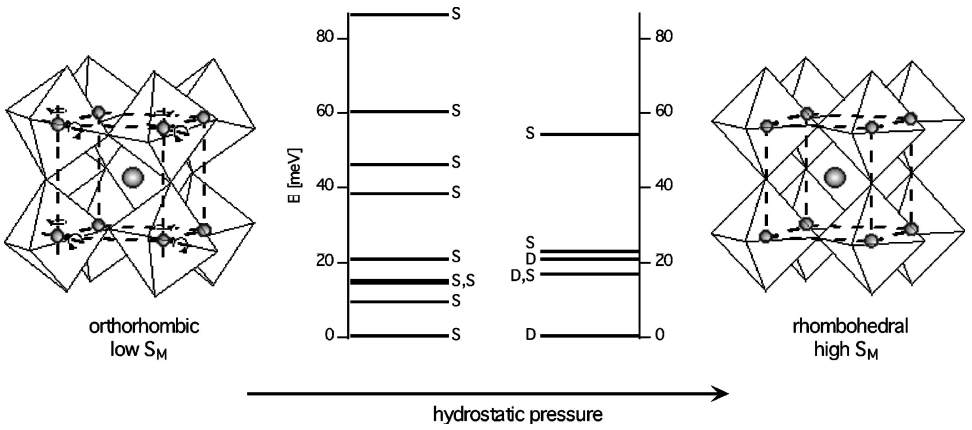

FIG. 2. Structural phase transition in $Pr_xLa_{1-x}NiO_3$ with corresponding CEF splitting schemes.

for the change of S_m (S_{CEF}) have proved to lead to an effective cooling, as will be shown in Sec. III. The diversity in mechanisms leading to a BCE may be regarded as a specific feature of this kind of caloric effect that makes the BCE worthwhile to be studied not only from an applicative but also from a fundamental point of view.

III. EXPERIMENT

A. Structurally driven BCE

The rare-earth nickelate $Pr_xLa_{1-x}NiO_3$ represents the first compound studied for the occurrence of a BCE. It is also this compound for which the concept of cooling by adiabatic pressure application was first proposed by Müller *et al.*[5] The results on $Pr_xLa_{1-x}NiO_3$ are summarized briefly here. $Pr_xLa_{1-x}NiO_3$ is a perovskite system and undergoes a temperature-induced structural phase transition from orthorhombic $Pbnm$ ($T<T_{SPT}$) to rhombohedral $R\bar{3}c$ ($T>T_{SPT}$) space group. The transition temperature T_{SPT} may be tuned seamlessly by the Pr content x, and is found to shift to a lower temperature by the application of hydrostatic pressure [$T_{SPT}(x=1)\approx 700$ K, $dT_{SPT}/dx\approx 1000$ K, $dT_{SPT}/dp(x=0.5)\approx -50$ K/GPa,[5] $dT_{SPT}/dp(x=0.4)\approx -23(2)$ K/GPa (Ref. 8)]. Hence pressure-induced phase transitions $Pbnm \xrightarrow{p} R\bar{3}c$ may be realized over a temperature range up to 700 K at modest pressures (see Ref. 5 and references therein). The CEF splitting, and hence the magnetic entropy S_m, in orthorhombic and rhombohedral symmetry differ considerably[9] (Fig. 2) and allow for a pure structurally driven BCE.

BCE measurements have been carried out on $Pr_xLa_{1-x}NiO_3$ above room temperature[5] on $x=0.66$ and at low temperatures[10] on $x=0.5$ and 0.4. All measurements were carried out on bare powders and hydrostatic pressure. The BCE at temperatures above room temperature have yielded an effective cooling of a few 0.1 K for $p=0.5$ GPa in $Pr_{0.66}La_{0.34}NiO_3$ at $T=350$ K in competition with elastic heating[5] (note that the cooling by the BCE takes place while pressure is applied). For lower temperatures, where elastic contributions become less of a problem, the BCE has been found in competition to friction effects $\propto 1/C$, which are an inherent problem of powder samples.

Unfortunately, $Pr_xLa_{1-x}NiO_3$ must be synthesized under a high oxygen pressure. Up to now, only powder samples are available. It is concluded that efficient cooling is preferably achieved on ceramic or single-crystalline material.

B. Magnetically driven BCE

Pressure-induced magnetic cooling by use of a magnetic phase transition has been realized in two rare-earth monopnictides, namely CeSb and HoAs both crystallizing in a cubic NaCl structure (space group $Fm\bar{3}m$).[11–14]

1. CeSb

The CEF splitting in CeSb constitutes a doublet ground state with an excited quartet at ~ 40 K.[15] Despite its simple chemical structure CeSb shows one of the most complex magnetic phase diagrams ever found (Refs. 16 and 17, and references therein). Below $T_N\approx 16$ K antiferromagnetic ordering occurs in various magnetic phases with different stackings of ferromagnetic (001) planes with up (+) or down (−) spins along $\langle 001\rangle$ and paramagnetic planes (0). The first magnetic phase found below T_N with stacking sequence + − 0 is followed by at least 14 more experimentally observed magnetic phases before the system eventually realizes the AF-IA phase with + + − − sequence for $T<8$ K. All of these magnetic phase transitions are found to be of first order. The free energy and thus the magnetic entropy of the respective phases are almost indistinguishable as found, e.g., by an analysis of the specific heat peaks of the intra-magnetic transitions which are weak, if at all observable. Thus one may simplify the magnetic phase diagram into a magnetically ordered region for $T<T_N$ with correspondingly low S_m and a paramagnetic region with larger S_m. Uniaxial pressure along $\langle 001\rangle$ is found to increase T_N by $dT_N/dp=8$ K/GPa.[17] Therefore, uniaxial pressure applied at a temperature slightly above $T_N(p=0)$ may drive the system from the paramagnetic into the ordered state with correspondingly large Zeeman splitting of the CEF levels (Fig. 3). If applied isothermally this will result in a change of magnetic entropy ΔS_m, i.e., in an extensive caloric effect. Subsequent adiabatic release of pressure will bring the system back into the paramagnetic phase involving an intensive caloric effect ΔT.

In Fig. 4 we show the schematic setup for the measurement of the BCE on single crystals under uniaxial pressure. The sample is placed on a socket. A piston transfers the uniaxial force onto the sample. The socket and the piston are

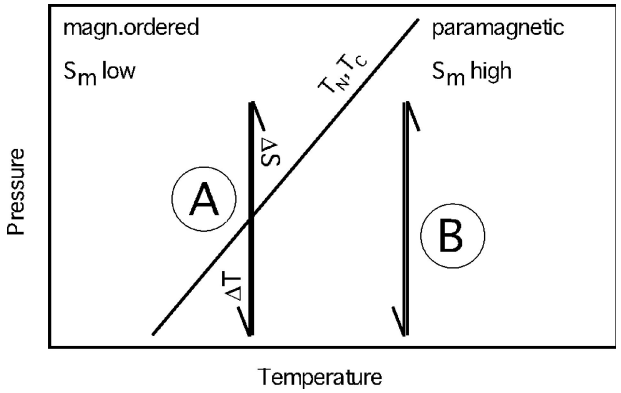

FIG. 3. Schematics for the magnetically driven BCE: only for (A) caloric effects ΔS, ΔT can be achieved, while for (B) the applied pressure is not sufficient to drive the system into the ordered state.

made from ZrO in order to minimize the thermal conductivity. A thin support disk of Teflon or tin (0.1 and 0.02 mm) reduces the risk of crushing the sample. The temperature evolution is tracked by a Au/Fe thermocouple glued on one of the free surfaces of the sample. Typical sample sizes were $2.5\times2.5\times2.5$ mm^3.

Figure 5 shows the measured T dependence of the intensive BCE ΔT for $p=0.26$ GPa. A representative time-evolution of the sensor temperature $T(t)$ is shown in the inset of Fig. 5. As expected, the fast pressure release is associated with a drop in temperature. A maximum cooling of -2 K could be observed upon a pressure release of $p=0.52$ GPa. Due to the thermal connection with the socket and the piston, $T(t)$ eventually relaxes back to the initial temperature. The temperature dependence of ΔT is characterized by a triangular shape.

The observed BCE may be calculated by means of the adiabatic equation (4) with the total entropy modelled according to Hamiltonian (16) with

$$\hat{\mathcal{H}}_{\mathrm{CEF}}=B_4^0(\hat{O}_4^0+5\hat{O}_4^4). \tag{21}$$

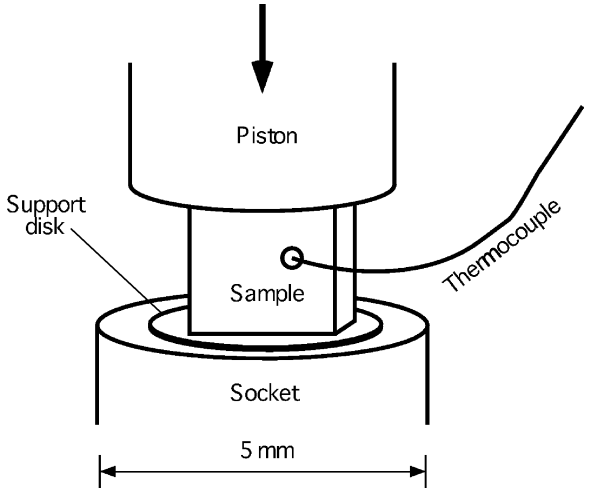

FIG. 4. Setup for the measurement of the BCE under uniaxial pressure.

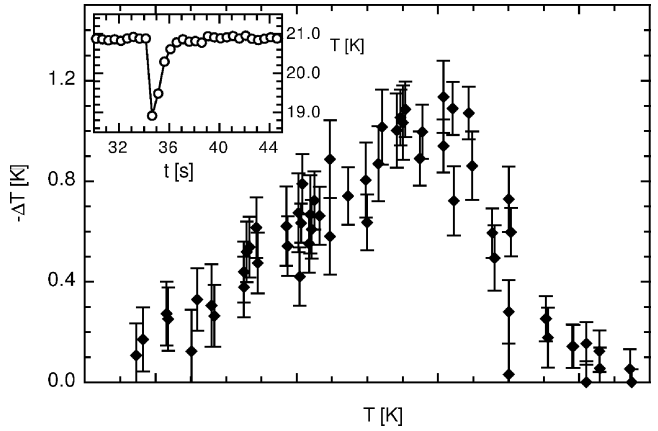

FIG. 5. Temperature dependence of the observed intensive BCE in CeSb for $p=0.26$ GPa $\|[001]$. Inset: Evolution of the sensor temperature upon a pressure release of $p=0.52$ GPa.

Figure 6 shows the modeled entropy curves at ambient and elevated pressure together with the resulting intensive BCE. The parameters used for this calculation are listed in Table I. The CEF parameter B_4^0 is taken from Ref. 15, and assumed to be independent of pressure. The mean-field parameters λ_D and λ_Q at ambient pressure are chosen to match (i) $T_N(p=0)$, (ii) $S(T)$ at $p=0$ resulting from integration of the measured c_p data (gray line, Fig. 6), (iii) the magnetic moment of Ce^{3+} as measured by neutron diffraction.[18] γ is taken from Ref. 19 and β is extrapolated from the Debye temperature of other monopnictides.[20,21] Both values are assumed to be pressure independent. Hence elastic heating/cooling is neglected in accordance with the experimental findings. The two mean-field parameters for $p>0$ are adjusted to reproduce the pressure-dependence of the ordering temperature $dT_N/dp=8$ K/GPa (Ref. 17) and a pressure-independent magnetic entropy S_M for $T<T_N(p=0)$. The latter criterion comes from the facts that (i) the magnetic phases below T_N are energetically almost indistinguishable, and (ii) no cooling effect below $T_N(p=0)$ can be observed experimentally [i.e., $S(p=0)\simeq S(p>0)$].

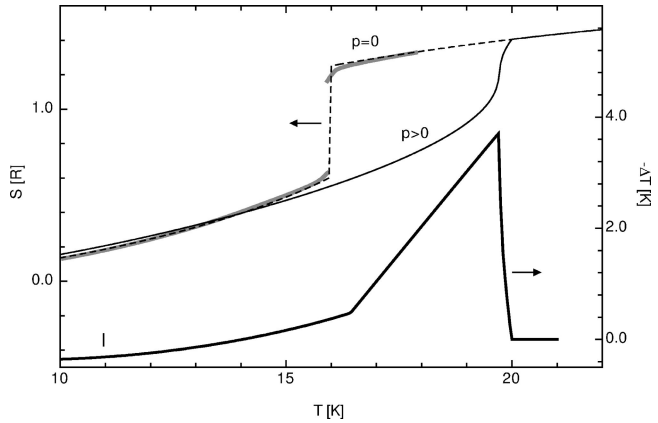

FIG. 6. Calculated entropy curves and resulting intensive BCE in CeSb. The gray line in the upper curve represents the total entropy S from integration (13) of experimental c_p values at ambient pressure.

TABLE I. Parameters for the model of the BCE in CeSb (Fig. 6).

p (GPa)	$B_4^0\times10^2$ (meV)	λ_D (μeV)	λ_Q (μeV)	$\beta\times10^3$ [R/K^3]	$\gamma\times10^6$ [R/K]
0	0.89	524	37.0	2.4	1.35
$\approx$0.26	0.89	690	30.5	2.4	1.35

The calculated BCE satisfies the experiment except for a factor 2.5 for the magnitude of the BCE. The value of the maximum ΔT is expected to be about the difference of the two ordering temperatures $T_N(p=0)$ and $T_N(p>0)$. Subsequent BCE experiments on $Ce_3Pd_{20}Ge_6$ have revealed that corrections due to the heat load of the temperature sensor and due to the thermal conductivity between sample and its environment are well necessary. These correction factors arising from the dynamics of the thermometry may well be as large as 3 (see the Appendix). Unfortunately, the low sampling rate (2 meas./sec) did not allow for the application of these corrections. The pressure dependence of the mean-field parameters λ_D and λ_Q shown in Table I are in accordance with the $p-T$ phase diagram. Especially the tendency of λ_Q to become smaller with pressure is consistent with a weakening of the quadrupolar order eventually driving the system at the critical end point into the AF-I phase.[17]

Finally it is worthwhile to address two comments on the pressure dependence of the (paramagnetic) CEF in CeSb, which is completely neglected in the above model. Uniaxial pressure is expected to distort the structure of the crystal. Correspondingly the CEF cannot be described in cubic symmetry. The tetragonal distortion results in an additional small term $\propto B_2^0\hat{O}_2^0$ in Hamiltonian (21). As a consequence the quartet at $\sim$40 K is split into two doublets. Note however, that any change in symmetry cannot split the CEF levels into more than doublet states, as Ce^{3+} constitutes a Kramers ion ($J=5/2$). Thus the ground state remains unchanged. The splitting of the quartet will have a negligible influence on the magnetic entropy S_m due to its low thermal population at $T<20$ K. Similarly, a pressure dependence on B_4^0 will only shift the quartet slightly keeping S_m almost constant for $T<20$ K. Hence at low temperatures the change of S_M results almost entirely from the Zeeman effect upon the ground-state doublet of CeSb and the above made approximations neglecting the pressure-effect on the (paramagnetic) CEF are well justified.

2. HoAs

HoAs orders below $T_N=4.4(1)$ K in the antiferromagnetic type-II structure with the moments aligned along the cube edges.[22,23] As for most of the rare-earth monopnictides pressure is expected to increase T_N.[24] The cubic CEF causes the J ground-state multiplet of Ho^{3+} to be split into a $\Gamma_3^{(2)}$ ground-state doublet, a $\Gamma_4^{(2)}$ triplet at 0.20 meV, and a Γ_1 singlet at 0.63 meV. The remaining 11 CEF states are more than 9 meV above the ground-state level, and hence do not contribute to the magnetic entropy at low temperatures.[14]

Figure 7 shows the directly observed BCE as a function of initial temperature for a pressure release up to 0.3 GPa $\|[001]$. The maximum cooling increases almost linearly with pressure and is shifted to higher temperatures T. At higher pressures a pronounced shoulder at the high temperature side appears up to around 18 K. Note that these shoulders spread out well into a temperature region where the sample is supposed to stay in the paramagnetic state at any given time and thus cannot result from a magnetically driven BCE (Fig. 3, case B).

As opposed to the case of CeSb, the nature of Ho^{3+} being a non-Kramers ion allows the magnetic entropy of HoAs to be more sensitive upon a change in structure. Indeed the observed ΔT within the paramagnetic state may be ascribed to the additional splitting of the CEF states due to tetragonal distortion induced by the uniaxial pressure as is shown in the following. Based on the elastic constants c_{ij} the tetragonal distortion $t=(c-a)/a=\Delta(c/a)$ may be calculated:

$$t=-\frac{c_{11}+2c_{12}}{c_{11}^2+c_{11}c_{12}-2c_{12}^2}p. \tag{22}$$

With values c_{ij} found from literature for other monopnictides (ErSb, PrSb, YbAs),[25] one yields $t\approx-0.8\%$/GPa. Based on the extended point-charge model including screening effects of the CEF by conduction electrons we may parametrize the nondistorted (cubic) case and extrapolate the CEF splitting in the distorted (tetragonal) case. The change in symmetry causes the appearance of a non-zero B_2^0 parameter and the release of the relations $B_4^4=5B_4^0$, $B_6^4=-21B_6^0$ valid for cubic symmetry only. Details of this calculation are given elsewhere.[14] The CEF parameters for the cubic and tetragonal case are listed in Table II, the resulting splitting schemes together with the associated entropies are depicted in Fig. 8. Under tetragonal distortion the ground-state doublet $\Gamma_3^{(2)}$ is

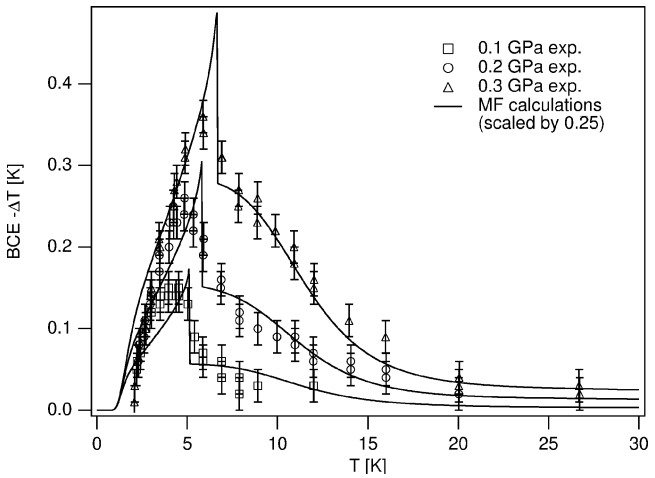

FIG. 7. Measured BCE in HoAs together with a model calculation (CEF parameters from Table II).

TABLE II. Model parameters for the BCE in HoAs as shown in Figure 7 ($t=0$: CEF parameters from inelastic neutron scattering (Ref. 14), $t>0$ values from extended point-charge model calculations) (all values in meV).

t [%]	$B_2^0\times10^3$	$B_4^0\times10^4$	$B_4^4\times10^3$	$B_6^0\times10^7$	$B_6^4\times10^6$	T_N (K)	$\lambda_D\times10^3$	$\lambda_Q\times10^6$
0		−3.02(5)		−3.87(30)		4.4(1)	15.2	20
−0.2	−0.72	−3.03	−1.52	−3.94	8.27	5.9	19.3	20
−0.3	−1.09	−3.04	−1.52	−3.99	8.35	6.7	20.5	20

split into two separate singlet states and the triplet state $\Gamma_4^{(2)}$ into a singlet and a doublet. The resulting magnetic entropy [Eq. (15)] is significantly reduced and hence explains the BCE above the Néel point (Fig. 8 and inset). The resulting intensive BCE ΔT can now be calculated by use of Eq. (4) with the lattice and electronic entropies modeled as described in Sec. II B. Specifically, we have used $\Theta_D=230$ K extrapolated from non-magnetic LaAs and LuAs[26] and $\gamma \approx 10$ mJ/K^2 mol.[19,26] Both contributions are only weakly pressure dependent and elastic heating may well be neglected in this temperature range. The solid line in Fig. 7 shows the best fit, which well explains the shape of the BCE −except close to the magnetic phase transition temperature, where fluctuation phenomena must be considered too. As in the case of CeSb the observed values of the BCE are considerably smaller than the calculated ones (i.e., in Fig. 7 the calculation has been downscaled by 0.25 to fit the observed data). Note that the present data acquisition rate (20 meas./sec) did not allow for corrections due to the dynamics of the measurement as was done in the case of the BCE in $Ce_3Pd_{20}Ge_6$ (see Sec. IV and the Appendix).

C. BCE in a Kondo system

In Kondo compounds it is generally found that the hybridization between the $4f$ and conduction electrons leads to a reduction of magnetic entropy as experienced experimentally, e.g., by an analysis of specific heat data and described empirically, e.g., by the resonance-level model proposed by Schotte and Schotte.[27] In the metallic Kondo compound $Ce_3Pd_{20}Ge_6$ (space group $Fm\bar{3}m$) this reduction in S_m is significant, as the two crystallographic Ce^{3+} sites both constitute a quartet CEF ground-state with an excited doublet state at $\Delta_{CEF}=60$ and 46 K, respectively.[28] The magnetic entropy associated to the quartet ground-state $S_Q=R\ln 4$ is not reached until $T=10$ K, far within the paramagnetic region of the compound ($T_Q=1.25$ K, $T_N=0.75$ K). The observed hybridization is strong with a linear specific heat term γ up to 8 J/(mol Ce K^2).[29,30] The application of pressure is expected to influence the magnetic entropy twofold: (i) a reduction of cell volume is generally found to increase the degree of $4f$-sd hybridization,[31,32] and (ii) uniaxial pressure leads to a structural distortion, so that the quartet ground-state is split into two doublets. Both effects will reduce S_m and thus allow for a BCE.[33]

Figure 9 shows the observed cooling effect upon uniaxial pressure release along $\langle 111\rangle$. No significant BCE ΔT is observed for temperatures $T\gtrsim 10$ K, where the full magnetic entropy is recovered. On the other hand for $T<10$ the apparent ΔT express directly the sensitivity of S_m upon uniaxial pressure. A maximum ΔT of −0.75 K at 4.4 K and 0.3 GPa could be observed. Note that these values have been cor-

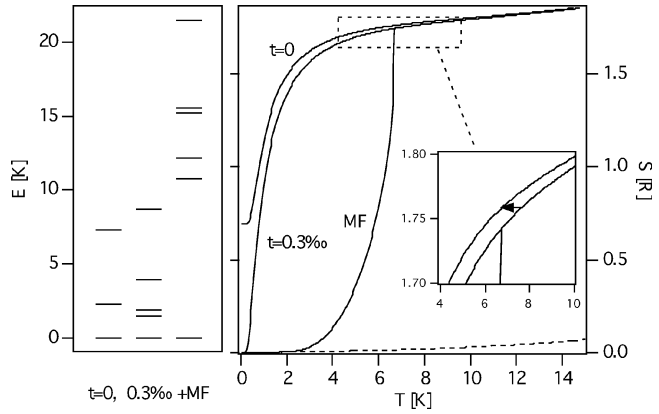

FIG. 8. Left: expected CEF scheme of HoAs under the influence of tetragonal distortion and molecular field (six lowest levels only). Right: calculated total entropies in HoAs for the nondistorted $t=0$, distorted $t=-0.3\%$, and Zeeman split cases with $t=-0.3\%$ (dashed line: nonmagnetic entropy). Due to the distortion, cooling above T_N is possible (arrow in inset).

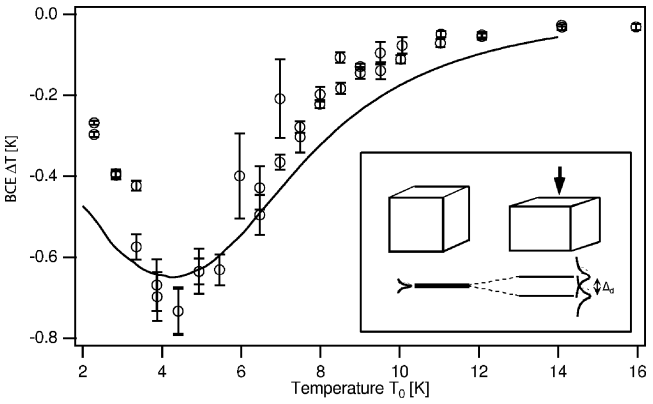

FIG. 9. Experimentally determined and calculated temperature dependence of the BCE in $Ce_3Pd_{20}Ge_6$ for a pressure release of $p=0.3$ GPa as a function of initial temperature T_0 (values for calculation listed in Table III). The experimental data are corrected for the dynamics of the thermometry and reflect ΔT in Eqs. (A7) and (A8) (Appendix). A representative temperature evolution is shown in Fig. 14 (Appendix). The inset shows schematically the effects of uniaxial pressure: (i) a tetragonal distortion leading to a splitting of the ground-state quartet, and (ii) a broadening of the CEF states due to strengthened hybridization.

TABLE III. Model parameters for the BCE in $Ce_3Pd_{20}Ge_6$ [β (mJ/mol Ce K^4) and γ (mJ/mol Ce K^2)]. Δ_{CEF} corresponds to the weighted average CEF splitting of both Ce^{3+} sites.

p [GPa]	γ(La)	β(La)	$\delta\gamma$	Δ_{CEF} (K)	Δ_K (K)	Δ_d (K)
0	506(7)	2.57(5)	15(3)	52	0.54(2)	0
0.3	506(7)	2.57(5)	15(3)	52	0.66(2)	−0.4(2)

rected for the dynamics of the temperature sensor (see the Appendix), while for the previous measurements on CeSb and HoAs these corrections could not be applied.

As in the previous examples the modeling of $S(T,p)$ allows for the calculation of the BCE via Eq. (4). While the nonmagnetic part S_N of the total entropy may be taken from specific heat data of $La_3Pd_{20}Ge_6$ by Kitagawa *et al.*[29] and written $S_N=\gamma(\mathrm{La})T+\beta(\mathrm{La})/3T^3$, the magnetic part may be expressed as $S_m=\delta\gamma T+S_{\tilde{\mathrm{CEF}}}$, where $\delta\gamma$ reflects the enhanced linear term in C and $S_{\tilde{\mathrm{CEF}}}$ the reduced CEF entropy. The latter may be expressed within the resonance-level model proposed by Schotte and Schotte.[27] In the nondistorted case the quartet ground state may be treated as an effective $S=3/2$ system, while in the distorted case the quartet is split into two doublet states with $S=\pm 1/2$ and $S=\pm 3/2$. The free energy due to the CEF is hence given by

$$F_{\tilde{\mathrm{CEF}}}=-kT\int_{-\infty}^{\infty}\frac{(\Delta_K/\pi)d\epsilon}{\epsilon^2+\Delta_K^2}\ln\left(\sum_{i=1}^{6}e^{-E_i/kT}\right), \qquad (23)$$

with

$$E_{1,2}=-\frac{\Delta_d}{2}\pm\frac{1}{2}\epsilon,$$

$$E_{3,4}=+\frac{\Delta_d}{2}\pm\frac{3}{2}\epsilon,$$

$$E_{5,6}=\Delta_{\mathrm{CEF}},$$

where Δ_K and Δ_d expresses the degree of $4f$-sd hybridization with a value of the same order as the Kondo energy kT_K and the splitting of the ground-state quartet, respectively, and where $E_{5,6}$ are included for the sake of completeness (these two states are hardly affected by the hybridization).

Starting from the values for γ(La) and β(La) taken from $La_3Pd_{20}Ge_6$, we may fit Δ_K and $\delta\gamma$ from specific heat data of $Ce_3Pd_{20}Ge_6$ at $p=0$. These values reflect $S(T,p=0)$, and are listed in Table III. The effect of uniaxial pressure upon the degree of hybridization and the splitting of the CEF level is associated to a change in Δ_K and Δ_d, respectively. The values found in order to describe the observed BCE are listed in Table III with the corresponding temperature dependence of the BCE shown in Fig. 9. Uniaxial pressure of 0.3 GPa is thus found to increase the degree of $4f$-sd hybridization by about 20% with a simultaneous splitting of the ground-state quartet by about −0.4 K. At temperatures $T<3$ K the model overestimates the BCE, as it does not take into account short range order effects of the quadrupolar and dipolar magnetic moments.

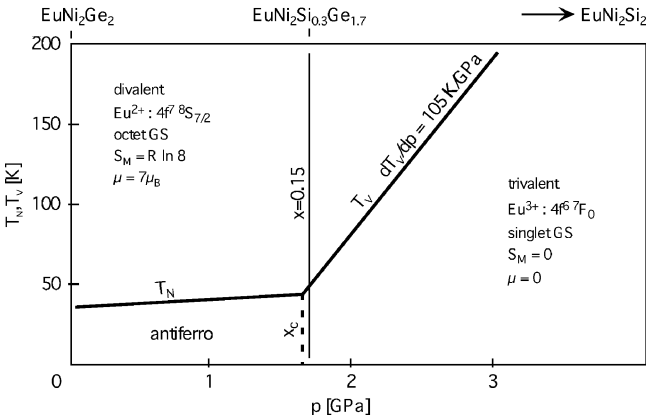

FIG. 10. Generalized x-T and p-T phase diagram of $EuNi_2(Si_xGe_{1-x})_2$ (Refs. 36 and 37).

D. Valence driven BCE

Valence transitions represent another type of phase transition well-known to exhibit a strong pressure dependence due to the different radii of the ion in the respective valence states. Eu compounds are especially well suited for a valence driven BCE, as the change from divalent magnetic Eu^{2+} to trivalent nonmagnetic Eu^{3+} implies drastic changes in the magnetic entropy. Among the Eu compounds with an intermediate valence regime and a strongly temperature dependent valence, $EuNi_2(Si_xGe_{1-x})_2$ shows a very sharp and almost complete valence transition.[34] In the ternary compounds $EuNi_2Ge_2$ and $EuNi_2Si_2$, the Eu ion is found in the magnetic divalent ($4f^7\ {}^8S_{7/2}$) and nonmagnetic trivalent ($4f^6\ {}^7F_0$) states, respectively. Both compounds crystallize in the tetragonal $ThCr_2Si_2$ structure type (space group $I4/mmm$). The compounds $EuNi_2(Si_xGe_{1-x})_2$ exhibit Eu^{2+} ions with antiferromagnetic ordering for $T<40$ K at Si concentration $x<x_c$ ($x_c\approx 0.15$), while for $x\geqslant x_c$ an intermediate valence regime with a strongly temperature dependent valence is observed. The hydrostatic pressure p was found to have the same effect as Si doping x, i.e., chemical pressure. Hence a generalized (x,p)-T phase diagram can be drawn for $EuNi_2(Si_xGe_{1-x})_2$ as shown in Fig. 10. The temperature-induced transition was found to be of first order for p close to the critical pressure and continuous for larger p. The pressure dependence of the valence transition temperature T_v is linear with $dT_v/dp=105$ K/GPa. X-ray-absorption spectroscopy measurements on $EuNi_2(Si_xGe_{1-x})_2$ estimated the mean valence of Eu to change from ≈ 2.2 to ≈ 2.85, for $x\approx 0.2$.[35]

The magnetic entropy difference $\Delta S_m=R\ln 8$ between the Eu^{2+} and Eu^{3+} state is amongst the largest to be realized practically (Eu^{2+}: $J=7/2\rightarrow$octet ground-state, $S=0\rightarrow$no CEF splitting; Eu^{3+}: $J=0\rightarrow$singlet ground-state). Note that $\Delta S_m=S_{3+\rightarrow 2+}=R\ln 8$ does not show any temperature dependence! Based on the Clausius-Clapeyron relation an entropy change $\Delta S\approx 18$ J/Kmol is estimated from the observed dT_v/dp value and the volume shrinkage of $\Delta V/V=-3.5\%$ below $T=T_v$.[36] The entropy change estimated by the analysis of specific heat measurements on $EuNi_2(Si_{0.15}Ge_{0.85})_2$ and $EuNi_2(Si_{0.125}Ge_{0.875})_2$ yields a slightly smaller value $\Delta S\approx 14.5$ J/Kmol.[37] The value $R\ln 8$ must be

considered as an overestimation because the mean valence values are found to be 2 and <3, respectively.

The BCE may be estimated in a similar way as done for all other compounds. The nonmagnetic entropy S_N may be estimated for $T<T_v$ from direct integration of c_p/T data taken at ambient pressure on $EuNi_2(Si_{0.15}Ge_{0.85})_2$. Note that for $T<T_v$ the Eu^{3+} is nonmagnetic. A fit to Eqs. (17) and (18) yields $\gamma=0.092(2)$ mJ/Kmol and $\Theta_D=265(5)$ K with the latter value in agreement with Mössbauer measurements [$\Theta_D(EuNi_2Ge_2)=300$ K and $\Theta_D(EuNi_2Si_2)=210$ K).[34] The magnetic entropy S_m may be modeled by a sigmoid function superimposed to S_N with $\Delta S_m=14.5$ J/Kmol and a width reflecting the experimental data at ambient pressure. The transition temperature may be assumed to change with $dT_v/dp=105$ K/GPa upon hydrostatic pressure. The change in S_N by pressure, i.e., elastic heating/cooling, is neglected. The resulting total entropy curves $S(T,p)$ are shown in Fig. 11 together with the expected extensive and intensive BCE. Already at modest pressures, an extensive and intensive BCE as large as 14.5 J/Kmol and -14 K, respectively, are expected over a considerable broad temperature range.

The BCE measurements on $EuNi_2(Si_{0.15}Ge_{0.85})_2$ were carried out in a pressure cell allowing for hydrostatic pressure.[38] The sample was cut into a cylindrical shape ($h=4.28$ mm, $m=350.3$ mg). Sodium chloride was used as the pressure transmitting medium. Figure 12 shows the effective cooling observed in function of temperature. A representative time-evolution of the measured temperature is shown in the inset of Figure 12. The observed cooling of the sample is clearly caused by the valence transition, as ΔT

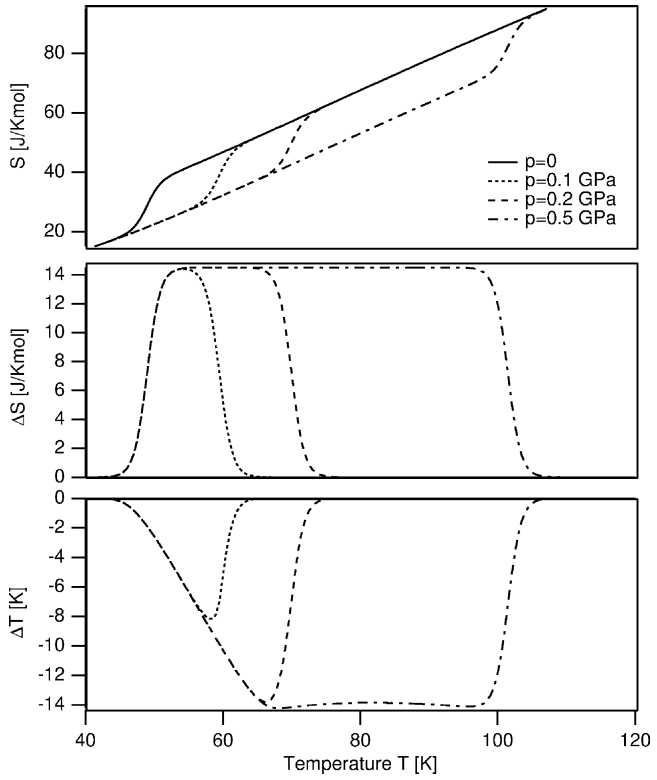

FIG. 11. Calculated total entropies and estimations for the expected true, extensive, and intensive BCE in $EuNi_2(Si_{0.15}Ge_{0.85})_2$.

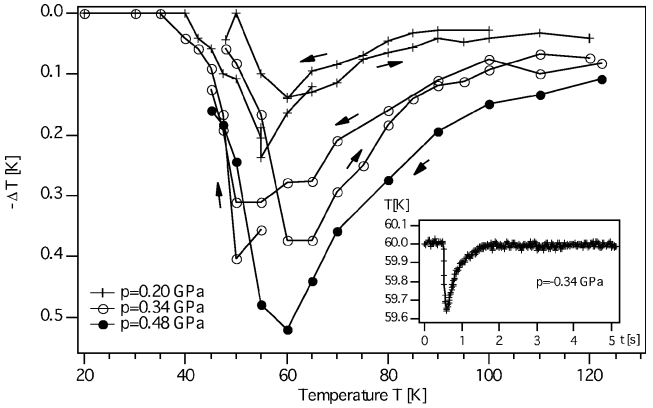

FIG. 12. Directly observed BCE in $EuNi_2(Si_{0.15}Ge_{0.85})_2$ (inset: representative time evolution of the temperature). Arrows denote the direction of measurement.

vanishes at the transition temperature $T_v(p=0)=38$ (48) K for cooling (warming) and decreases above about $T=80$ K [$\hat{=}\ T_v(p>0)$]. The cooling above 120 K is mostly caused by elastic heating from the pressure-transmitting medium and from the sample itself and to a lesser extent also from the BCE of the sample originating from pressures at the very edge of the pressure distribution (see below). The observed hysteresis may be explained by the first order nature of the valence transition. However, the directly observed BCE is found more than one order of magnitude smaller than expected from the estimation made above. The severe lack in adiabaticity of the hydrostatic setup is likely to be responsible for most of this reduction. Similar measurements on CeSb under hydrostatic pressure have revealed a reduction in ΔT of about a factor 14 ... 21 at 20 K, as compared with what is expected from calculations.[38] Thus the modest, observed values of ΔT do not necessarily contradict the above made estimations. While the non-adiabaticity is found to reduce $\Delta T(T)$ almost uniformly, it cannot explain the shape of the observed BCE deviating from what is expected (Fig. 11). Figure 12 clearly shows an effective cooling up to $T>80$ K for the $p=0.34$ and 0.48 GPa data sets, in agreement with dT_v/dp. Thus one may feel confident in the value of mean pressure acting on the sample. The deviation in shape of $\Delta T(T)$ is apparent if additional broadening of the transition for $p>0$ is considered too (Fig. 13). The use of a solid pressure medium is well expected to result in a nonuniform pressure distribution around the sample. In combination with the large pressure dependence of T_v, we may expect considerably broadened transitions for $p>0$ as well as to a lesser amount for $p=0$ due to remanent pressure. Note that differences in T_v and in the width of the transition were earlier ascribed to internal stress depending on the respective sample preparation technique.[34,35]

In spite of the strongly reduced ΔT, one may feel confident in the principle idea using a valence transition in Eu for pressure-induced magnetic cooling. Further improvements in the experimental setup or the use of single crystal samples will allow for the measurements of considerably larger ΔT.

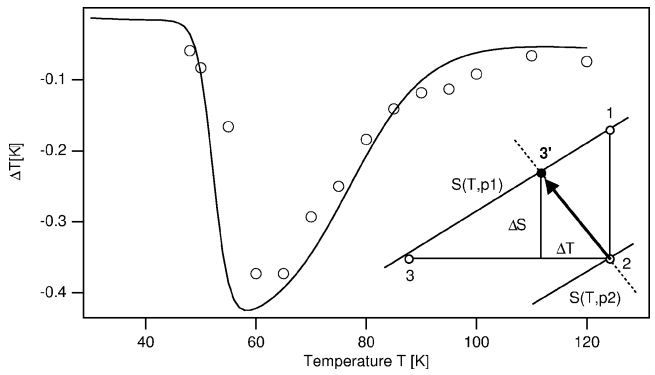

FIG. 13. Directly observed signal (open symbols) and estimation (line) to the $p=0.34$ GPa data set of the BCE in $EuNi_2(Si_{0.15}Ge_{0.85})_2$ (warming; see Fig. 12). The estimation assumes a non-adiabaticity $\eta\equiv[\Delta S/(\Delta S+\Delta T)]\approx 0.95$ and a substantial broadening of the transition at elevated pressure (broadened by a factor of 8 as compared to $p=0$). The drawing shows schematically the reduction of ΔT due to nonadiabaticity (in correspondence with Fig. 1).

IV. DISCUSSION

In the previous sections the BCE has been demonstrated on a variety of different compounds using different microscopic mechanisms to alter the magnetic entropy by pressure. The verification and understanding of these mechanisms make the study of this effect interesting *per se*, and may help for a better understanding of these compounds. We wish though to post some remarks with respect to a possible technical use of this effect in refrigerators. The close relation between the BCE and MCE urges to compare these two effects. As opposed to the MCE, little experimental data about the BCE is yet obtainable. In fact, the present work constitutes the first review on this topic, to our knowledge. The observed, intensive caloric effect ΔT is considerably reduced in the BCE as compared to what one may expect from calculations. This reduction is a direct consequence of the nonadiabaticity while measuring ΔT. Future experimental setups may improve this situation considerably, e.g., by use of piezo actuators for the force generation. Nevertheless nonadiabaticity remains an inherent problem of this new cooling technique, while for the MCE adiabatic conditions for the measurements of ΔT require less effort. The comparison between the intensive caloric effect in the BCE and MCE, respectively, must also be discussed in context of indirect determinations as often applied for the estimation of the MCE. These are based on measurements of $\partial M/\partial T(H)$ via a Maxwell relation or on specific heat data at $H>0$ and $H=0$ (see Sec. II A). In fact, the majority of MCE data found in the literature is determined in this way. The invalidity of the analogous Maxwell relation for the BCE and the inaccessibility of quantitative specific heat data for $p>0$ do not allow for the corresponding indirect determination of the BCE. Thus the intensive caloric effect ΔT represents the only variable which is directly accessible by the experiment.

The reduction of the observed intensive BCE ΔT must not be considered a primary obstacle for the technical use of the BCE. Present realizations of the MCE in magnetic refrigerators make use of the magnetic Stirling cycle proposed by Heer *et al.*[2] and Brown.[3] Basically, the adiabatic step $2\rightarrow 3$ (Fig. 1) is replaced by two steps along $S(T,X_2)$ and $S(T,X_1)$, respectively, while isothermal steps at the corresponding end points are used to pump heat from or to the refrigerator. As opposed to simple adiabatic cooling the proposed mechanism may be cycled. Technically, the steps along $S(T,X)$ are implemented by use of a regenerator. In the Ericsson-like magnetic refrigeration cycle the regenerator is a fluid in which the refrigerator is immersed in, while in the active magnetic refrigeration cycle the refrigerant itself constitutes the regenerator. The regenerator provides a temperature gradient along which $S(T,X)$ is varied $(2\rightarrow 3)$. In turn the heat deposition and assimilation at the respective end points of the gradient, which result from the isothermal steps, further feed the gradient. Thus the temperature gradient within the regenerator increases with every cycle until eventually heat losses and the limited working range of the refrigerant (see below) saturate it. At present we see no principal hindrance which would not allow for an implementation of a Stirling cycle using the BCE.

The primary factor, which determines the capacity of heat pumped with the above cycle, is the extensive caloric effect ΔS (per mass of refrigeration material). Thus we may briefly compare ΔS obtained in BCE and MCE materials, respectively. In CeSb and $EuNi_2(Si_{0.15}Ge_{0.85})_2$ the extensive caloric effect accounts for $\Delta S=0.6R=5$ J/Kmol$\sim$19 J/Kkg and $\Delta S=14.5$ J/Kmol$\sim$39 J/Kkg with modest pressures of $\sim$0.2 GPa, respectively. These values may well be put in relation to Gd with $\Delta S\sim 9$ J/Kkg at $\Delta B=5$ T and to giant MCE compounds like $Gd_5(Si_{1.72}Ge_{2.28})$ and $MnFeP_{0.45}As_{0.55}$ both with $\Delta S\sim 18$ J/Kkg at $\Delta B=5$ T, respectively.[39]

Another factor limiting the practical use of a refrigerator material represents its working range Γ, i.e., the temperature span for which $\Delta S>0$. While this span is restricted to a few K in the case of CeSb, HoAs and $Ce_3Pd_{20}Ge_6$, it may reach very large values in a valence driven BCE. Note that $\Delta S_{2+\rightarrow 3+}$ in Eu is principally not temperature dependent, thus the working range of $EuNi_2(Si_xGe_{1-x})_2$ is solely limited by the shift in T_v (Fig. 11). At pressures of $p=0.5\,(0.2)$ GPa, extensive caloric effects ΔS over a temperature span of $\Gamma=50\,(20)$ K can be realized [compare to e.g., $Gd_5(Si_{1.72}Ge_{2.28})$ and $MnFeP_{0.45}As_{0.55}$ both with $\Gamma=30\,(12)$ K for $\Delta B=5\,(2)$ T].[39]

V. CONCLUSIONS

External pressure has been found an effective tool to alter the magnetic entropy of some rare-earth compounds. The associated extensive and intensive caloric effects (ΔS and ΔT) have been demonstrated for $Pr_xLa_{1-x}NiO_3$, CeSb, HoAs, $Ce_3Pd_{20}Ge_6$, and $EuNi_2(Si_{0.15}Ge_{0.85})_2$. The underlying microscopic mechanisms resulting in a pressure-induced change of the magnetic entropy include structural or/and magnetic phase transitions, hybridization effects in Kondo compounds and valence transitions. Both caloric effects ΔS and ΔT could be modeled based on microscopic properties of the compounds. The obtainable extensive caloric effects ΔS are compared to corresponding values found for the MCE. The size and the temperature span of ΔS in

$EuNi_2(Si_xGe_{1-x})_2$ may well be compared with the best known MCE materials. The study of the BCE on other compounds may reveal a better understanding of their respective thermodynamic and magnetic properties. The practical importance of the BCE is subject to further studies of this new issue.

ACKNOWLEDGMENTS

We thank K. A. Müller for stimulating discussions. We are indebted to K. Mattenberger, A. Dönni and T. Komatsubara for cooperation at the early stage of this project and for providing us the single crystal samples. The expert technical assistance of S. Fischer, R. Thut, M. Zolliker, and P. Häberli is gratefully acknowledged.

APPENDIX

A closer look at the evolution of the measured temperature $T(t)$ reveals that T does not drop down instantaneously but continuously and that this relaxation is distinctly slower than the time needed for the release of pressure (Fig. 14). Eventually $T(t)$ relaxes back to the temperature of the environment T_0. The evolution of the sensor temperature T_1 may be described within a simple model depicted in the inset of Fig. 14. The sample (1) stays in contact with the sensor (2) and the environment (0) via effective thermal conductivities η_{12} and η_{10}. The environment acts as a heat sink (i.e., $Q_0 \rightarrow \infty$). The BCE is assumed to cause an instantaneous drop ΔT in the sample temperature. The temperatures of the sample and sensor then obey

$$\dot{T}_1(t) = \frac{1}{C_1}\{\eta_{12}[T_2(t) - T_1(t)] + \eta_{10}[T_0 - T_1(t)]\}, \tag{A1}$$

$$\dot{T}_2(t) = \frac{1}{C_2}\{\eta_{12}[T_1(t) - T_2(t)]\}, \tag{A2}$$

with C_1 and C_2 the specific heats of the sample and the sensor, respectively. The exact solutions for $T_1(0) = T_0 + \Delta T$ and $T_2(0) = T_0$ are

$$T_1(t) = T_0 + \Delta T e^{-(b/2)t}\left[\cosh\frac{\sqrt{D}}{2}t - \frac{a_{10} + a_{12} - a_{21}}{\sqrt{D}}\sinh\frac{\sqrt{D}}{2}t\right], \tag{A3}$$

$$T_2(t) = T_0 + \Delta T\frac{2a_{21}}{\sqrt{D}}e^{-(b/2)t}\sinh\frac{\sqrt{D}}{2}t, \tag{A4}$$

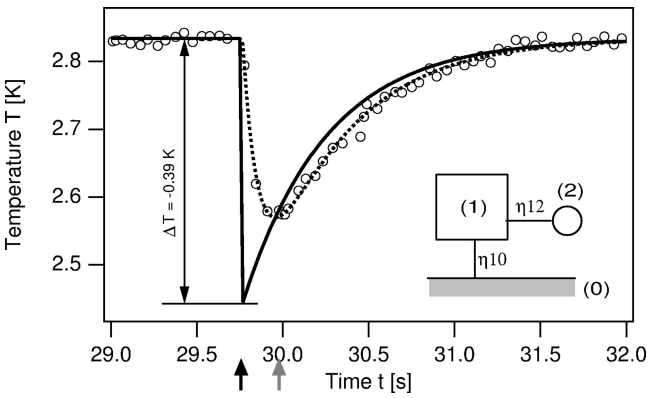

FIG. 14. Observed temperature evolution (circles) together with fitted evolutions for the sensor and sample temperature $T_2(t)$ and $T_1(t)$ in $Ce_3Pd_{20}Ge_6$ at a pressure release of 0.3 GPa $\|[111]$ (see Sec. III C). Inset: schematic heat conduction model (0: environment, 1: sample, 2: sensor).

and $a_{10} = \eta_{10}/C_1$, $a_{12} = \eta_{12}/C_1$, $a_{21} = \eta_{12}/C_2$, $b = a_{10} + a_{12} + a_{21}$, and $D = b^2 - 4a_{10}a_{21}$. The parameter a_{21} can be associated with the heat load of the sensor. The measured temperature evolutions may now be fitted in Eq. (A2) yielding a_{ij} and the true, though not directly measurable cooling of the sample ΔT. The evolution of the true sample temperature may be then reconstructed via Eq. (A3). In practice the fits in Eq. (A4) have proved to be unstable with large correlations between the fitting parameters. Hence the model may be simplified by assuming T_1 to relax exponentially, the heat flow from the sample to the sensor and the environment is then combined to an effective thermal conductivity $\tilde{\eta}_{10}$. The twodifferential equations (A1) and (A2) reduce to

$$\dot{T}_1(t) = \frac{\tilde{\eta}_{10}}{C_1}[T_0 - T_1(t)], \tag{A5}$$

$$\dot{T}_2(t) = \frac{\eta_{21}}{C_2}[T_1(t) - T_2(t)], \tag{A6}$$

with solutions ($T_1(0) = T_0 + \Delta T$, $T_2(0) = T_0$),

$$T_1(t) = T_0 + \Delta T e^{-t/\tau_1}, \tag{A7}$$

$$T_2(t) = T_0 + \Delta T\frac{\tau_1}{\tau_1 - \tau_2}[e^{-t/\tau_1} - e^{-t/\tau_2}] \tag{A8}$$

where the two relaxation constants are $\tau_1 = C_1/\tilde{\eta}_{10}$ and $\tau_2 = C_2/\eta_{12}$. The resulting curves $T_1(t)$ and $T_2(t)$ are essentially indistinguishable from Eqs. (A3) and (A4) within the parameter range of interest ($\tau_2 \ll \tau_1$). The fitting of the experimental data in Eq. (A8) can now be donewithout numerical difficulties and yields the true BCE ΔT as wellas the evolution of the sample temperature $T_1(t)$ (Fig. 14).

*Present address: Physique des Milieux Condensés, Université Pierre et Marie Curie B77, 4 Place Jussieu, 75252 Paris, France. Electronic address: thierry.strassle@pmc.jussieu.fr

[1] A.M. Tishin, in *Handbook of Magnetic Materials*, by K.H.J. Buschow (Elsevier, Amsterdam, 1999), Vol. 12.

[2] C.V. Heer, C.B. Barnes, and J.G. Daunt, Rev. Sci. Instrum. **25**, 1088 (1954).

[3] G.V. Brown, J. Appl. Phys. **47**, 3673 (1976).

[4] V.K. Pecharsky and K.A. Gschneidner, Jr., J. Magn. Magn. Mater. **200**, 44 (1999).

[5] K.A. Müller, F. Fauth, S. Fischer, M. Koch, A. Furrer, and Ph. Lacorre, Appl. Phys. Lett. **73**, 1056 (1998).
[6] V.K. Pecharsky and K.A. Gschneidner, Jr., J. Appl. Phys. **86**, 565 (1999).
[7] V.K. Pecharsky and K.A. Gschneidner, Jr., J. Appl. Phys. **90**, 4614 (2001).
[8] Th. Strässle *et al.*, ILL experimental report, CRG-376 (D1A) (2000).
[9] S. Rosenkranz *et al.*, Phys. Rev. B **60**, 14 857 (1999).
[10] Th. Strässle, Master's thesis, Eidgenössische Technische Hochschule Zürich, 1999.
[11] Th. Strässle, A. Furrer, Ph. Lacorre, and K.A. Müller, J. Alloys Compd. **303-304**, 228 (2000).
[12] Th. Strässle and A. Furrer, High Press. Res. **17**, 325 (2000).
[13] Th. Strässle, A. Furrer, and K.A. Müller, Physica B **276-278**, 944 (2000).
[14] Th. Strässle, A. Furrer, F. Altorfer, K. Mattenberger, M. Böhm, and H. Mutka, J. Alloys Compd. **323-324**, 392 (2001).
[15] H. Heer, A. Furrer, W. Hälg, and O. Vogt, J. Phys. C **12**, 5207 (1979).
[16] T. Chattopadhyay, P. Burlet, J. Rossat-Mignod, H. Bartolin, C. Vettier, and O. Vogt, Phys. Rev. B **49**, 15 096 (1994).
[17] B. Hälg, A. Furrer, and O. Vogt, Phys. Rev. Lett. **21**, 2745 (1986).
[18] G. Meier, Ph.D. thesis, Institut für Reaktortechnik ETHZ, AF-SSP-105, 1977.
[19] T. Kasuya, Y.S. Kwon, T. Suzuki, K. Nakanishi, F. Ishiyama, and K. Takegahara, J. Magn. Magn. Mater. **90**, 389 (1990).
[20] R.J. Birgeneau, E. Bucher, J.P. Maita, L. Passell, and K.C. Turberfield, Phys. Rev. B **8**, 5345 (1973).
[21] N. Wakabayashi and A. Furrer, Phys. Rev. B **13**, 4343 (1976).
[22] B. Schmid, P. Fischer, and F. Hulliger, J. Less-Common Met. **111**, 191 (1985).
[23] F. Hulliger, in *Handbook on the Physics and Chemistry of Rare Earths*, edited by K.A. Gschneidner, Jr. *et al.* (North-Holland, Amsterdam, 1979), Vol. 4.
[24] F.P. Missell, R.P. Guertin, and S. Foner, Solid State Commun. **23**, 369 (1977).
[25] M.E. Mullen, B. Lüthi, P.S. Wang, E. Bucher, L.D. Longinotti, J.P. Maita, and H.R. Ott, Phys. Rev. B **10**, 186 (1974).
[26] A. Aeby, F. Hulliger, and B. Natterer, Solid State Commun. **13**, 1365 (1973).
[27] K.D. Schotte and U. Schotte, Phys. Lett. A **55**, 38 (1975).
[28] L. Keller, W. Henggeler, and A. Furrer, Europhys. Lett. **26**, 353 (1994).
[29] J. Kitagawa, N. Takeda, and M. Ishikawa, Phys. Rev. B **53**, 5101 (1996).
[30] A. Dönni, T. Hermannsdörfer, P. Fischer, L. Keller, F. Fauth, K.A. McEwen, T. Goto, and T. Komatsubara, J. Phys.: Condens. Matter **12**, 9441 (2000).
[31] J.A. Blanco, M. Podesta, J.I. Espeso, J. Sal, C. Lester, K.A. McEwen, N. Patrikios, and J. Fernandez, Phys. Rev. B **49**, 15 126 (1994).
[32] C.D. Bredl, F. Steglich, and K.D. Schotte, Z. Phys. B: Condens. Matter **29**, 327 (1978).
[33] Th. Strässle, A. Furrer, A. Dönni, and T. Komatsubara, J. Appl. Phys. **91**, 8543 (2002).
[34] G. Wortmann, I. Nowik, B. Pertscheid, G. Kaindl, and I. Felner, Phys. Rev. B **43**, 5261 (1991).
[35] H. Wada, A. Nakamura, A. Mitsuda, M. Shiga, T. Tanaka, and H. Mitamura, J. Phys.: Condens. Matter **9**, 7913 (1997).
[36] H. Wada, M.F. Hundley, R. Movshovich, and J.D. Thompson, Phys. Rev. B **59**, 1141 (1999).
[37] Z. Hossain (private communication).
[38] Th. Strässle, Ph.D. thesis, Swiss Federal Institute of Technology ETH, Zurich, 2002, http://e-collection.ethbib.ethz.ch/show?type=diss&nr=14707
[39] O. Tegus, E. Brück, K.H.J. Buschow, and F. de Boer, Nature (London) **415**, 150 (2002).